Electronic Supplementary Material (ESI) for Energy & Environmental Science.

A Solvent Molecule Reconstruction Strategy Enabling a High-Voltage Ether-based Electrolyte

Xudong Peng,[a ‡] Tianshuai Wang,[a ‡] Bin Liu,[a] Yiju Li,[a,b,c,*] Tianshou Zhao[a,b,*]

[a] *Department of Mechanical and Aerospace Engineering, The Hong Kong University of Science and Technology, Clear Water Bay, Kowloon, Hong Kong SAR, China*

[b] *Department of Mechanical and Energy Engineering, Southern University of Science and Technology, Shenzhen, 518055, China*

[c] *The HKUST Jockey Club Institute for Advanced Study, The Hong Kong University of Science and Technology, Clear Water Bay, Kowloon, Hong Kong SAR, China*

[*] Corresponding author. E-mail: zhaots@sustech.edu.cn (T.S. Zhao).

[*] Corresponding author. E-mail: liyj6@sustech.edu.cn (Yiju Li).

[‡] These authors contributed equally to this work.

1. Calculation Details

1.1 Molecule dynamic simulations.

All molecule dynamic (MD) simulations were performed by the GROMACS 2018.8 simulation package with the amber99sb-ildn force fields [1,2]. We generated the atomic charges of anions and solvent molecules by the restrained electrostatic potential fitting procedure (RESP) evaluated at the B3LYP/6-311G+(d,p) carried out with the Gaussian 09 package and the Multifwn software [3]. Topology files and bonded and Lennard-Jones parameters were generated by using the Sobtop[4]. Herein, an oligomer ($[C_2H_5OCH_2O]_3H$) form was utilized to simplify the polymer electrolyte simulations. The equilibrium and production simulations were calculated in the NPT ensemble at constant pressure (1.01325 bar) and temperature (298.15 K) in a cubic box with periodic boundary conditions in all *xyz* Cartesian direction. For equilibrium processes, the temperature is maintained by V-rescale coupling with a time constant of 0.2 ps. The Berendsen barostat was adopted for controlling pressure, which is with a coupling constant of 0.5 ps. Equilibrium simulation ran 5 ns. For production simulation, the V-rescale coupling and parrinello-rahman barostat were used to control the temperature and pressure, respectively. Production simulation ran 20 ns (2fs per step, simulating $1*10^7$ steps) for obtaining the equilibrium Li^+ coordination shell structure at room temperature for electrolytes. Electrostatic interactions were treated using the Particle-Mesh-Ewald (PME) method [5]. The coordination number of molecules of type i in the first solvation shell surrounding a single molecule of type j is calculated as:

$$N_i = 4\pi n_j \int_0^{R_M} g_{ij}(r) r^2 dr$$

In which R_M is the distance of the first minimum following the first peak in the radial distribution function (RDF), $g_{ij}(r)$, which is a standard approach for bulk liquid. All the visualizations of MD simulation were implemented by VMD software. Solvation shell statistics were calculated by using the MDAnalysis Python package [6] by histogramming the observed first solvation shells for lithium ions during the production simulation using a method similar to Yu's work [7-8].

1.2 Ab-initial calculations

All the computational simulations of LUMO/HOMO were performed on the basis of DFT calculations with a plane-wave technique which is implemented in the Vienna ab initio simulation package (VASP) [9]. Gradient corrected exchange-correlation functional of Perdew, Burke, and Ernzerhof (PBE) models were used under the projector augmented wave (PAW) method [10], with a cut-off kinetic energy of 500 eV for plane-wave basis. The convergence criterion of the total energy was set up to be within 1×10^{-5} eV, while all the atoms and geometries were optimized until the residual forces became less than 1×10^{-2} eV/Å. Visualization of the structures was performed by the VESTA (Visualization for Electronic and Structure Analysis).

2. Experimental Details

2.1 Electrolyte preparation

The LiFSI salt was purchased from DodoChem (Suzhou) Ltd. The NCM622 (single crystal) was purchased from Guangdong Canrd New Energy Technology Co. Ltd. All the other reagents and chemicals for electrolyte preparation were bought from Sigma-Aldrich. The "m" in this work means molar salt in liter solvent, while "M" stands for molar salt in liter solution (here, we do not include the volume of TTE). The 2.6 M LiTFSI-DOL-TTE, 1.3 M LiTFSI+1.3 M LiFSI-DOL-TTE, and Hybrid-DOL/PDOL-TTE in this work were all prepared by dissolving the same amount of salt in the same amount of DOL solvents. The control electrolytes are named according to the approximate concentrations and prepared by simply dissolving salts with corresponding solvents. For example, the 2.6 M LiTFSI-DOL-TTE LiTFSI was prepared by dissolving 1.150 g (~4 mmol) LiTFSI in 1 mL DOL, followed by the addition of 1 mL TTE for dilution. The 1.3 M LiTFSI+1.3 M LiFSI-DOL-TTE is prepared by first dissolving 0.575 g LiTFSI salt into 1 mL DOL and then adding 0.375 g LiFSI, followed by the addition of 1 mL TTE for dilution. The Hybrid-DOL/PDOL-TTE was prepared through three steps: (1) The 0.375 g LiFSI salt was dissolved into 1 mL DOL to trigger the ring-opening reaction of DOL; (2) Then, 0.575 g LiTFSI salt was rapidly added into the above sticky and viscous solution followed by ten-minute stirring. The addition of LiTFSI helped reduce the viscosity, making the liquidus mixture more flowable; (3) 1 mL TTE was mixed with the above mixture and stirred for at least two hours to acquire the Hybrid-DOL/PDOL-TTE, which then stands for more than one week before use. All the above preparation steps were carried out in an Ar-filled glove box and under room temperature (~27 ℃), during which high temperature cases should be avoided.

2.2 Characterizations

For the postmortem analysis, all the cycled cathodes and anodes were directly retrieved from cells, then washed by DME, and dried for at least 12 hours. The NCM622 cathodes for postmortem analysis were retrieved after 50 cycles at 0.2 C in different electrolytes. The LMAs for postmortem analysis were cycled for 50 cycles using different electrolytes. A scanning electron microscope (SEM), JEOL-6700F, was used to acquire the morphologies of both fresh and cycled samples (both anodes and cathodes). X-ray photoelectron spectroscopy (XPS) was performed using a Physical Electronics PHI 5600 multi-technique system equipped with an Al monochromatic X-ray source. Time-of-flight Secondary Ion Mass Spectrometer (TOF-SIMS) tests with high ion detection sensitivity were carried out by TOF-SIMS V (ION-TOF GmbH), with a milling time

of 300 s, within an area of 30 μm×30 μm. The data of TOF-SIMS were further processed and visualized by ION-TOF software. Transmission electron microscopy (TEM) was used to observe the cycled NCM622 cathode particles (high-resolution JEOL 2010 TEM system with a LaB_6 filament at 200 kV). The focused ion beam (FIB) (FEI Helios G4 UX) was used for NCM622 particle cross-section analysis. The Raman spectra were obtained by InVia (Renishaw) MicroRaman/Photoluminescence System with a laser wavelength of 633 nm and wavenumber from 300 to 1200 cm^{-1}. Ionic conductivity tests of different electrolytes were performed by a symmetric configuration of stainless steels by CR2032 coin-cell. For each electrolyte, the conductivity was tested at least three times by discarding the severely deviated data. ^1H Nuclear Magnetic Resonance (NMR) spectra were acquired on a Bruker DPX 400 spectrometer at 400 MHz. To ensure the Hybrid-DOL/PDOL-TTE reaches a steady state, the electrolytes were placed for over one week before the NMR and the Raman characterizations.

2.3 Electrochemical performance

2.3.1 Coin cell tests

All the coin cells were assembled in the Argon-filled glove box with water and oxygen content lower than 0.1 ppm. Al-coated cathode cases with an additional Al-foil at the cathode side were used for all coin cells with NCM622 cathodes in this work. All the NCM622 were prepared by a blade-cast method (active cathode materials: super P: PVDF = 8:1:1), followed by calendar roll processes, and then punched into disks (ϕ=12 mm), with mass loadings of around 6.0 mg cm^{-2} for cell performance evaluation. The electrolyte volumes for each cell are about 60 μL. The LFP cathodes are prepared using similar routine as NCM622 cathodes with loadings around 4.5 mg cm^{-2}. The Celgard3501 Separator was used for all the cell tests if there is no special notation. For the 20 μm Li||NCM622 coin cells, 20 μm Li foil and a high-loading NCM622 cathode (20.5 mg cm^{-2} and 15.2 mg cm^{-2}, the ratios of components are NCM: Super P: PVDF = 90: 5: 5) were used. The tests were performed within the voltage range of 2.5-4.4V and 2.5-4.6V. Li foils (ϕ=12 mm, thickness = 450 μm) and Cu foils (ϕ=18 mm) were used for assembling the Li||Cu and Li||Li cells. The Li|Cu cells are first cycled at 0.1 mA cm^{-2} and 0.1 mAh cm^{-2} for 50 cycles before its cycling at 1 mA cm^{-2} and 1 mAh cm^{-2}.

2.3.2 Pouch cell tests (Li//NCM622 full cells)

The high-loading NCM622 cathodes for pouch-cell tests (20 μm Li|NCM622) were prepared with a ratio of NCM: Super P: PVDF = 85: 7.5: 7.5. The 5 mAh cm^{-2} Li||NCM622 pouch cell (4 cm× 5 cm) was tested with a cathode loading of 14.8 mg cm^{-2} (~3.0 mAh cm^{-2} at 0.05 C, N/P~1.7) within the voltage range of 2.5- 4.6 V. The 5 mAh cm^{-2} anode for pouch cell is electrodeposited in Li|Cu configuration using the electrolyte of 1 M

LiTFSI in DOL/DME (v/v =1:1) with 5 wt% $LiNO_3$. The electrolyte to the capacity ratio in pouch cells is around 4.0 g Ah^{-1} (11 mg cm^{-2} based on the cathode area). The electrolyte weight was measured by the weight difference of the pouch cell before and after adding the Hybrid-DOL/PDOL-TTE. The whole process of assembly and weight measurement was carried out in the Air-filled glove box. The pouch cell is evacuated using the vacuum sealer (MSK-115A-MS). Two bolts-anchored acrylic plates are used to control the pressure on the pouch cell during the tests.

All the above-mentioned galvanostatic charge-discharge (GCD) tests were operated using a Neware Battery Test System. The electrochemical impedance spectroscopy (EIS), from 1 MHz to 100 mHz with an amplitude of 5 mV, and cyclic voltammetry (CV), with a sweep rate of 0.2 mV s^{-1} were tested using a Biologic electrochemical workstation. A carbon-coated Al-foil (c-Al foil) serves as a working electrode with a sweep rate of 1 mV s^{-1} in the LSV tests. Round cycles from 2 to 5 V (vs. Li/Li^+) were carried out, and then the stable recorded cathodic scan for each Li|c-Al foil cells with different electrolytes were acquired as the LSV curve.

Figures and Tables

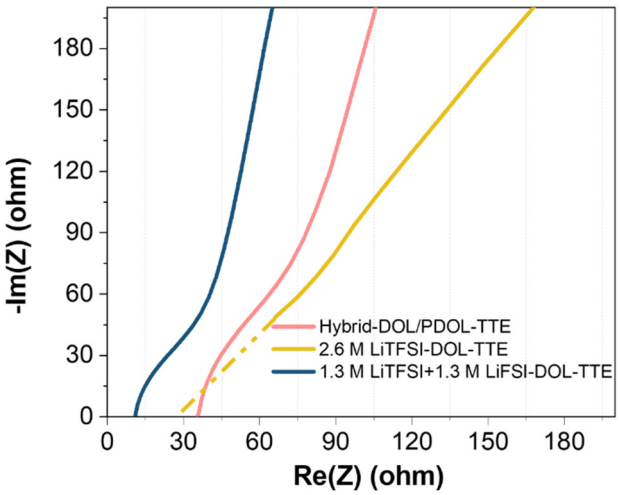

Figure S1. EIS plots of the SS|GF|SS cells (SS stands for the stainless steel, GF stands for the glass-fiber separator).

The thickness of the compressed GF is about 200 μm. Therefore, we could calculate the conductivities of electrolytes based on the following equation. The results are shown in **Table S1**:

$$\sigma = \frac{L}{RA}$$

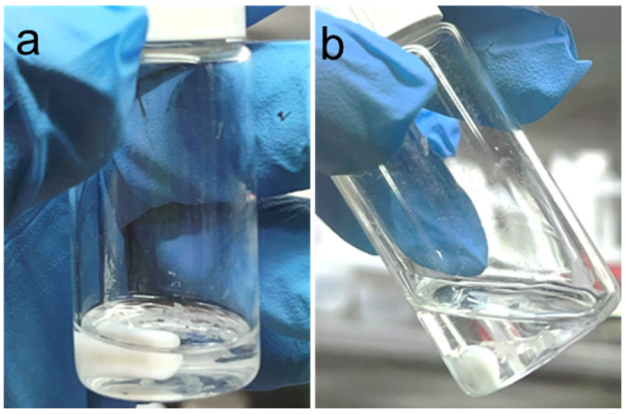

Figure S2. Photos of (a) the freshly prepared Hybrid-DOL/PDOL-TTE, and (b) the Hybrid-DOL/PDOL-TTE standing for three months.

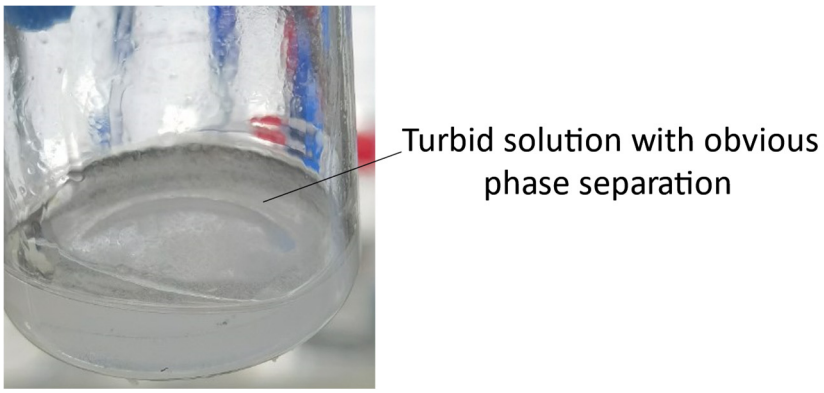

Figure S3. Digital image of 3 m LiFSI (~2 M) (first added) + 1 m LiTFSI (~0.6 M) in DOL-TTE after being placed for two weeks.

Figure S4. Digital image of 2 m (~1.3 M) LiFSI (first added) + 1 m (~0.6 M) LiTFSI in DOL-TTE after being placed for two weeks. This electrolyte shows a much higher viscosity than the Hybrid-DOL/PDOL-TTE. This comparison result illustrates the importance of the LiTFSI salt content.

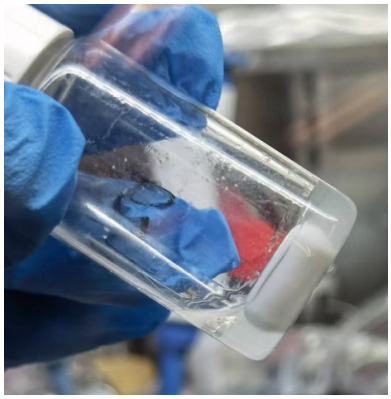

Figure S5. Digital image of 4 m LiFSI added to mixture of DOL-TTE after being placed for two weeks.

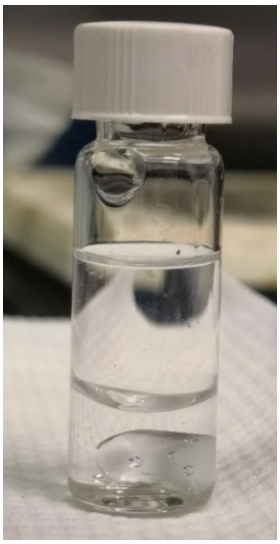

Figure S6. Digital image of the 2 m LiFSI triggered (fully polymerized for a long enough time) PDOL electrolyte (bottom) and TTE (top). The picture shows that the fully polymerized PDOL cannot be dissolved in the TTE, forming a solid-liquid separation state.

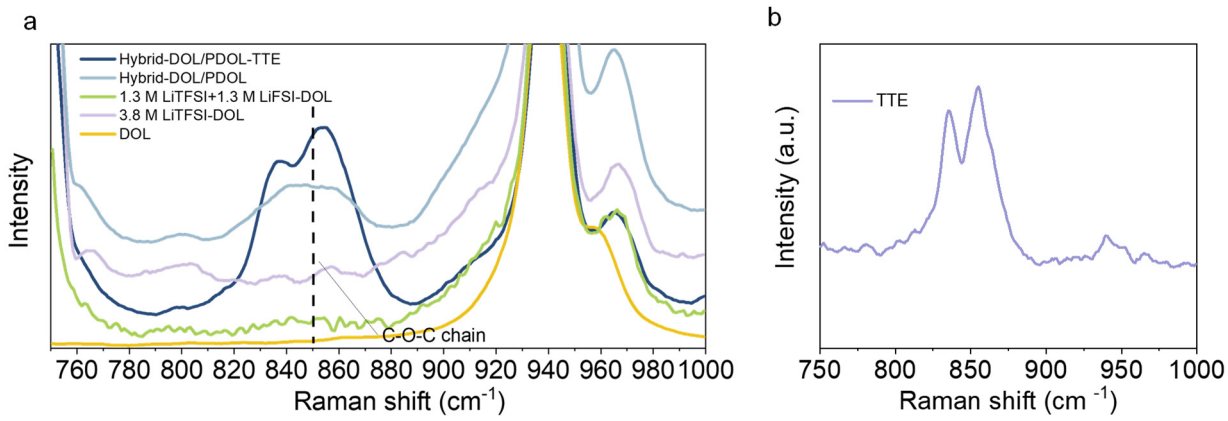

Figure S7. Raman spectra of (a) various electrolytes and (b) TTE. The peak of the C-O-C chain indicating existence of PDOL in Hybrid-DOL/PDOL-TTE.

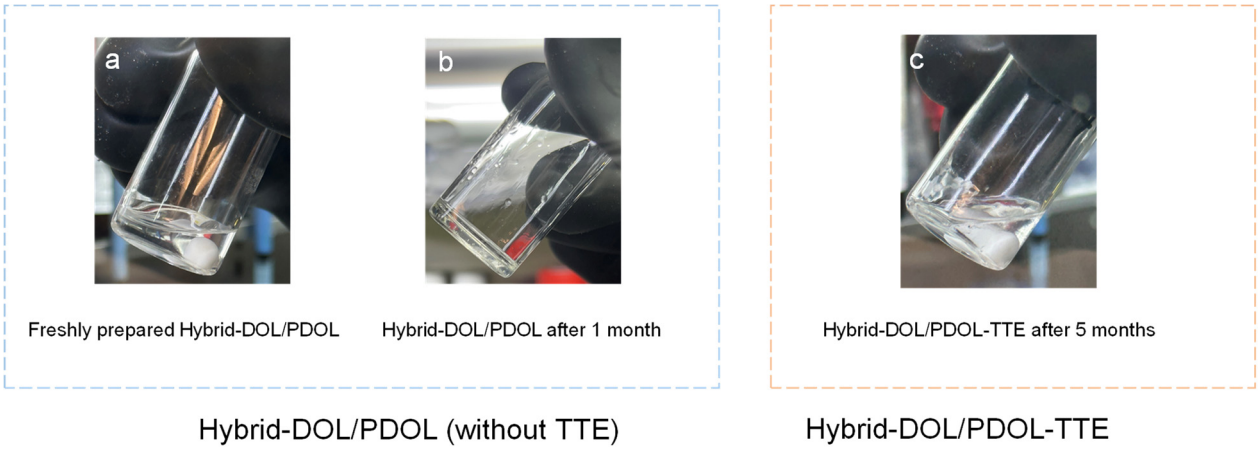

Figure S8. (a, b) Photos of the Hybrid-DOL/PDOL (without TTE) electrolyte and (c) Hybrid-DOL/PDOL-TTE electrolyte.

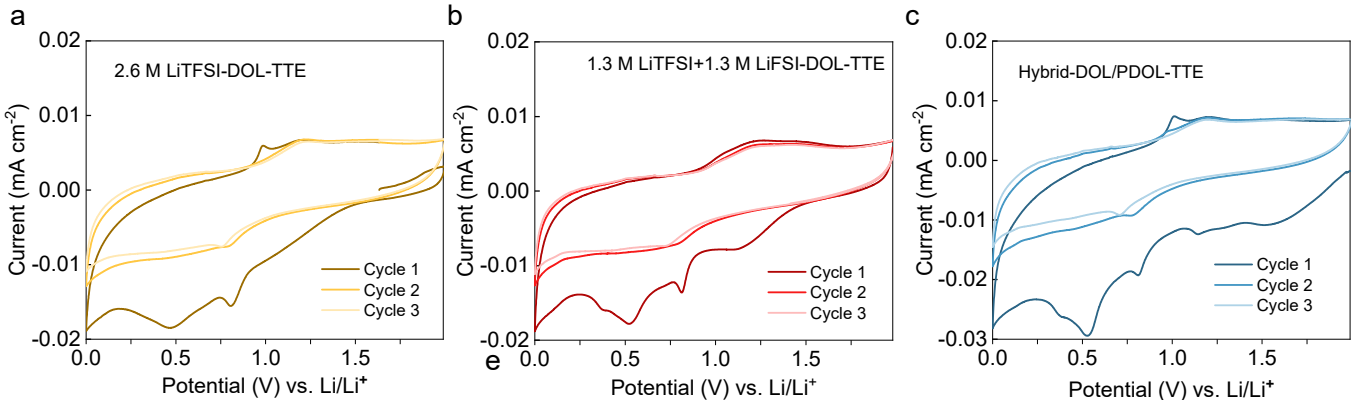

Figure S9. CV curves of Li|Cu cells using (a) 2.6 M LiTFSI-DOL-TTE, (b) 1.3 M LiTFSI+1.3 M LiFSI-DOL-TTE, and (c) Hybrid-DOL/PDOL-TTE.

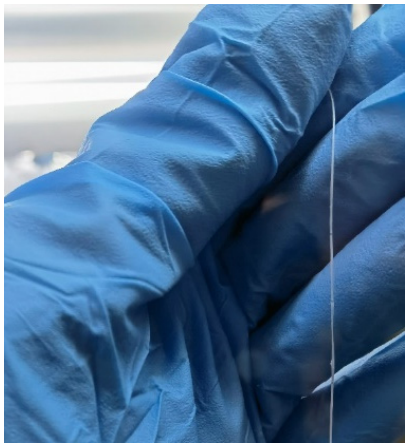

Figure S10. Photo image showing the residual of Hybrid-DOL/PDOL-TTE. A solid polymer remains after drying the Hybrid-DOL/PDOL-TTE at room temperature.

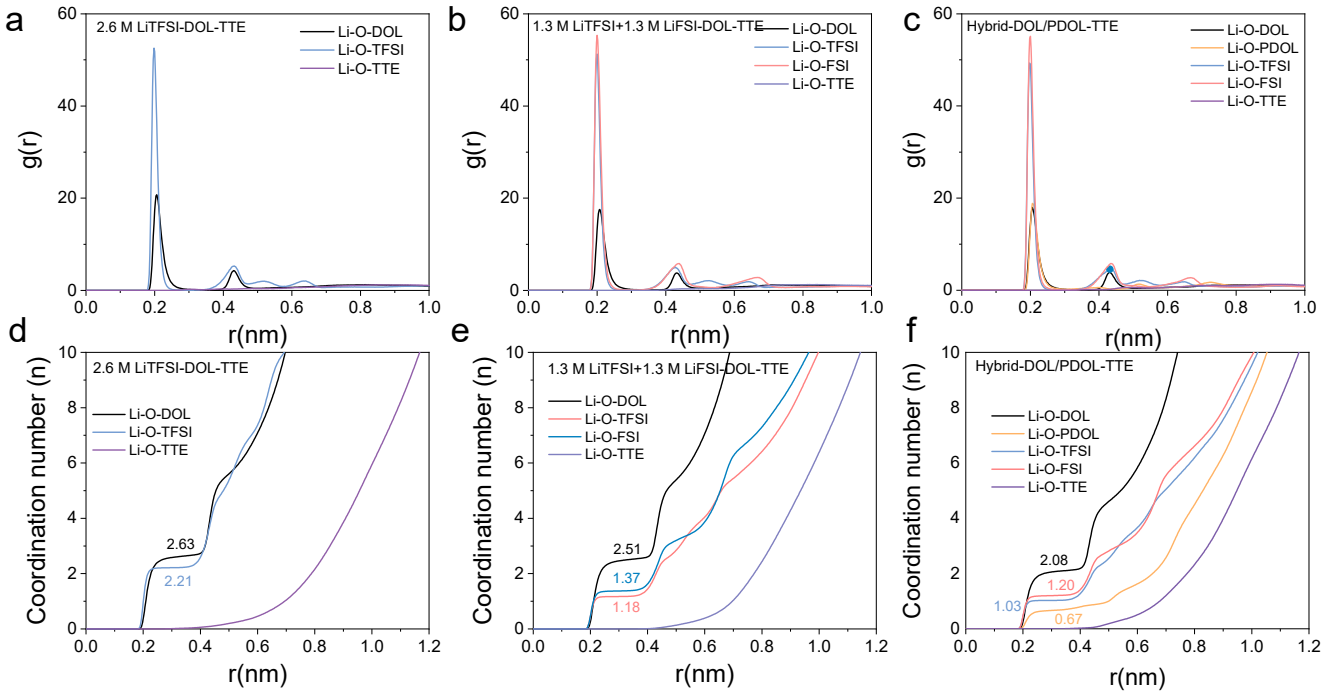

Figure S11. Radial distribution functions (RDFs) and coordination numbers (CNs) of the Li-ion in (a, d) 2.6 M LiTFSI-DOL-TTE, (b, e)1.3 M LiTFSI+1.3 M LiFSI-DOL-TTE, and (c, f) Hybrid-DOL/PDOL-TTE.

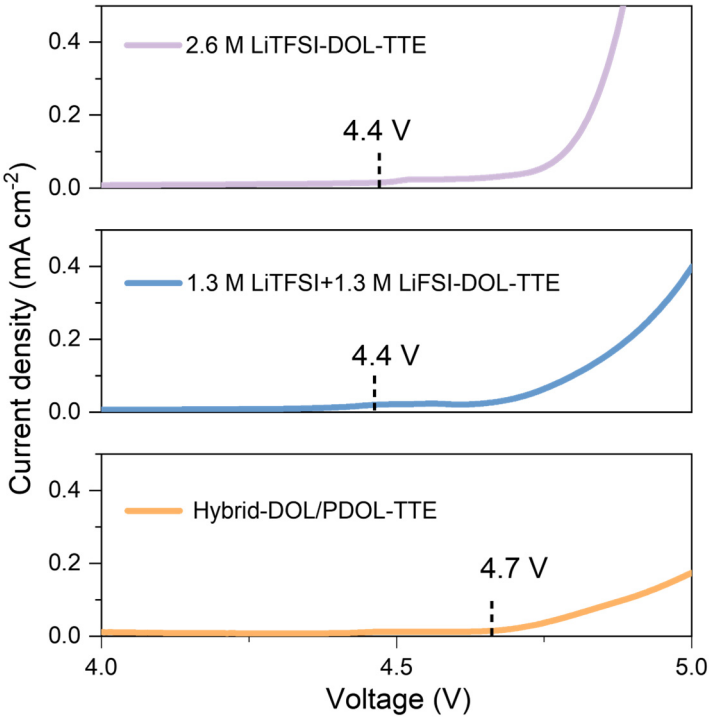

Figure S12. LSV curves of 2.6 M LiTFSI-DOL-TTE, 1.3 M LiTFSI+1.3 M LiFSI-DOL-TTE, and Hybrid-DOL/PDOL-TTE.

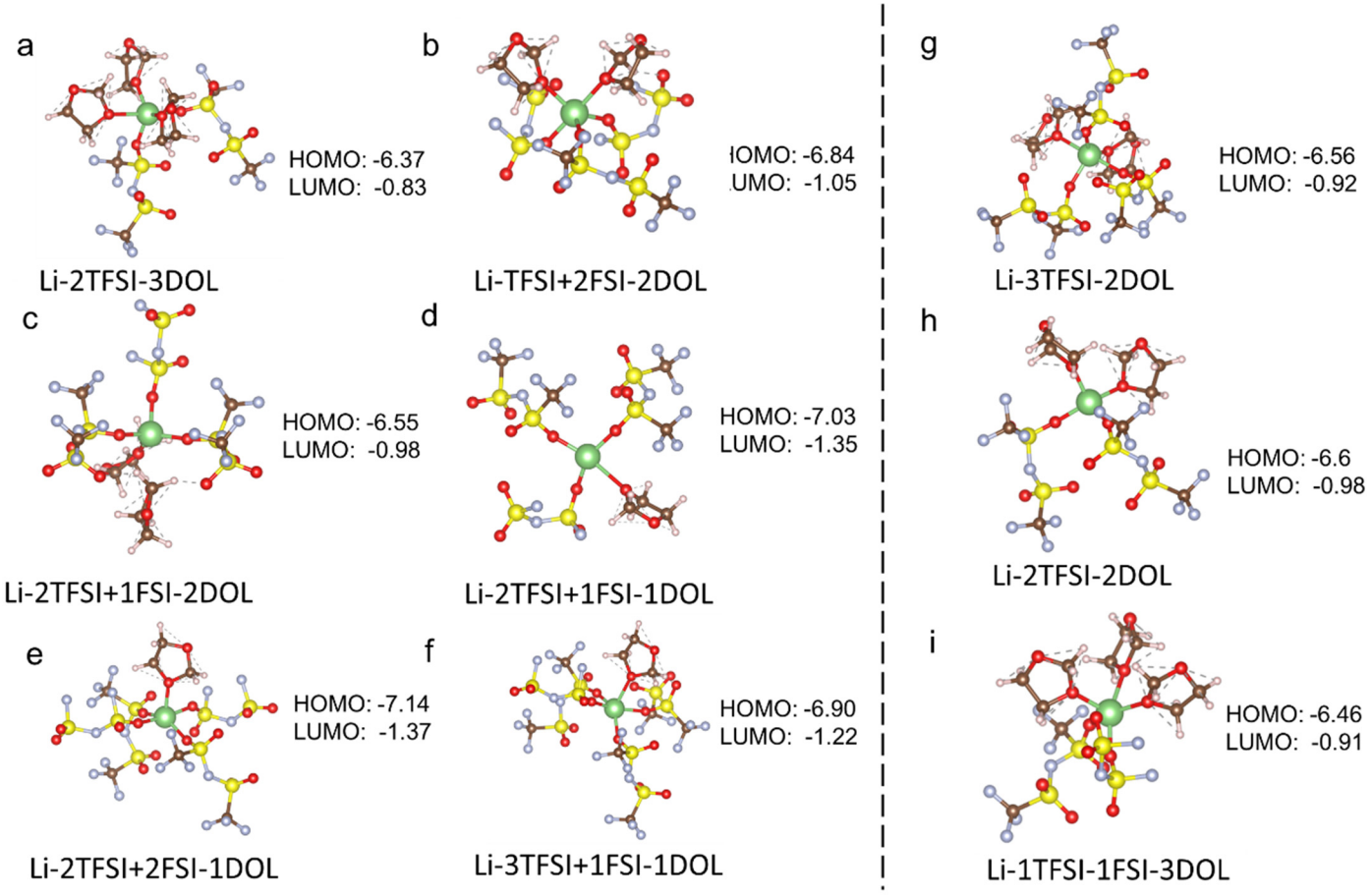

Figure S13. HOMO and LUMO energy levels of most probable ion-solvent configurations in the electrolytes of 2.6 M LiTFSI-DOL-TTE, 1.3 M LiTFSI+1.3 M LiFSI-DOL-TTE, and Hybrid-DOL/PDOL-TTE.

Through the DFT calculations of these frequent configurations in the electrolytes, all these configurations have a total coordination number (CN) ranging from 4-5. And there are several critical messages concluded easily. First, the FSI^- would lower the LUMO and HOMO more significantly compared to the $TFSI^-$ when the solvent molecules and total anion number are fixed (comparison between b & c, d & e, e & f, a & i, *etc*). Second, the number of DOL or the anion-solvent ratios (ASR) in the configuration has a significant impact on the LUMO and HOMO levels. Introducing one more DOL molecule could escalate the LUMO and HOMO (comparison between c & d, where one less DOL would reduce the LUMO by 0.48 eV and the HOMO by 0.37 eV). Based on these results, we summarized possible configurations with extremely low LUMO (**Table S4**). Therefore, we could know that the higher average number of FSI^- in the solvation sheath indicates the configurations with lower LUMO or HOMO. In this term, the Hybrid-DOL/PDOL-TTE has both the highest average number of FSI^- in the solvation sheath and the highest anion-DOL ratios according to the RDF results, which could be the reason why the Hybrid-DOL/PDOL-TTE has the strongest ability to passivate the anode and remain stable against oxidation compared to the other two electrolytes during long-term cycling.

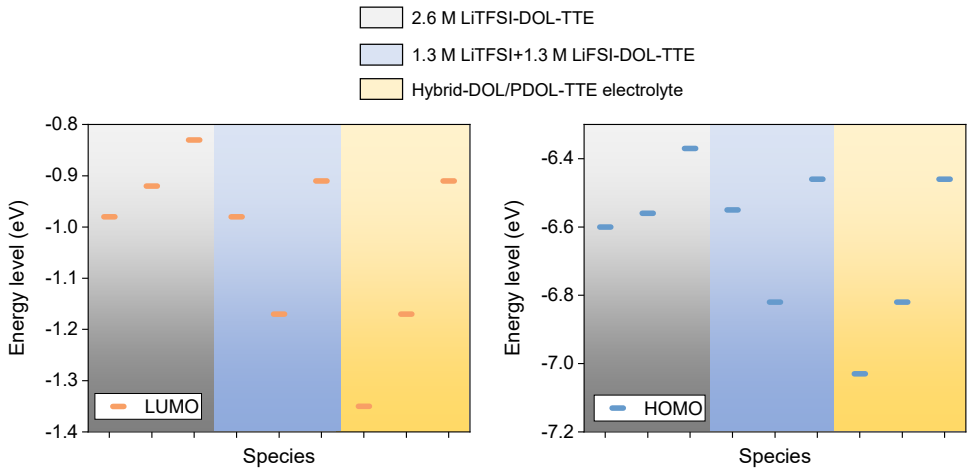

Figure S14. Plots of LUMO and HOMO energy levels of most frequent configurations in different electrolytes.

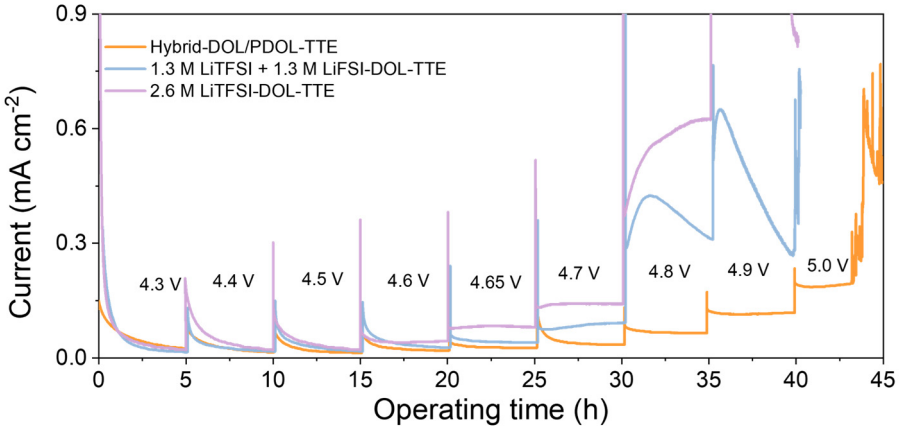

Figure S15. Floating analysis in Li|NCM622 cell configuration using different electrolytes.

The cells were previously cycled within 2.5-4.2 V. Step-by-step increased constant voltages were subsequently applied to the activated cells. The cells were held for 5 hours at each voltage plateau for measuring the stable leakage current. The 2.6 M LiTFSI-DOL-TTE shows the most significant leakage current above 4.3 V, and the current cannot be stabilized anymore when the voltage is increased to 4.6 V. The 1.3 M LiTFSI+1.3 M LiFSI-DOL-TTE shows obviously increased current densities after 4.65 V. By contrast, the Hybrid-DOL/PDOL-TTE shows a relatively lower leakage current and the leakage current at each voltage step remains stable till 4.9 V. These results further verify the excellent anti-oxidation ability of our Hybrid-DOL/PDOL-TTE and agrees with the results of the Li|NCM622 cell tests.

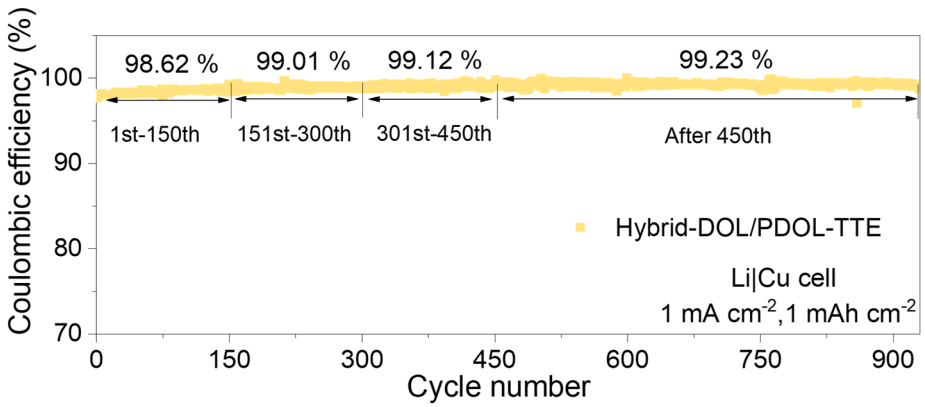

Figure S16. Cycling performance of Li|Cu cells using Hybrid-DOL/PDOL-TTE with specific average CEs in different ranges of cycle number (1st-150th, 151st-300th, 301st-450th, and after 450th).

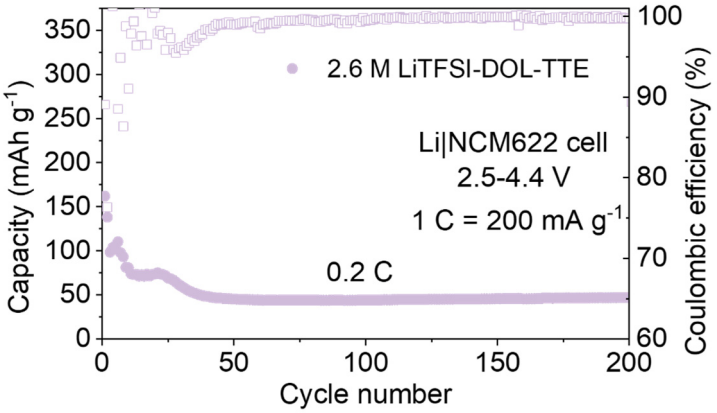

Figure S17. Cycling performance of the Li|NCM622 cell using 2.6 M LiTFSI-DOL-TTE (2.5-4.4 V).

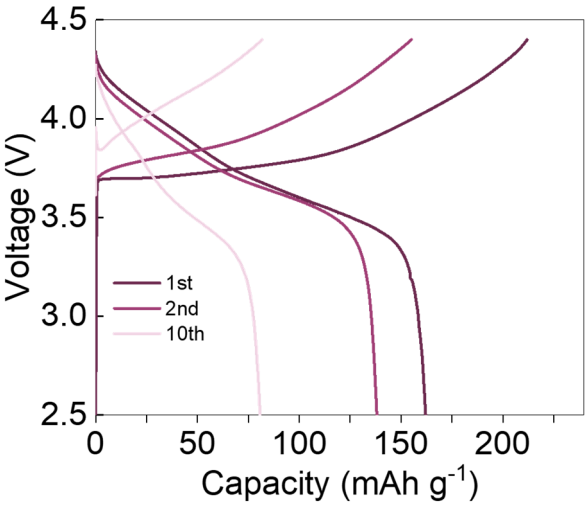

Figure S18. Voltage profile of the Li|NCM622 cell using 2.6 M LiTFSI-DOL-TTE at 0.2 C (2.5-4.4 V).

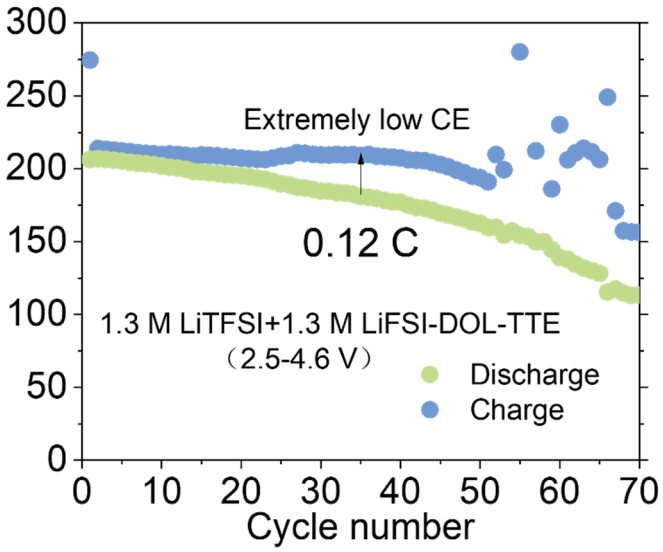

Figure S19. Cycling performance of the Li|NCM622 cell using 1.3 M LiTFSI+1.3 M LiFSI-DOL-TTE (2.5-4.6 V).

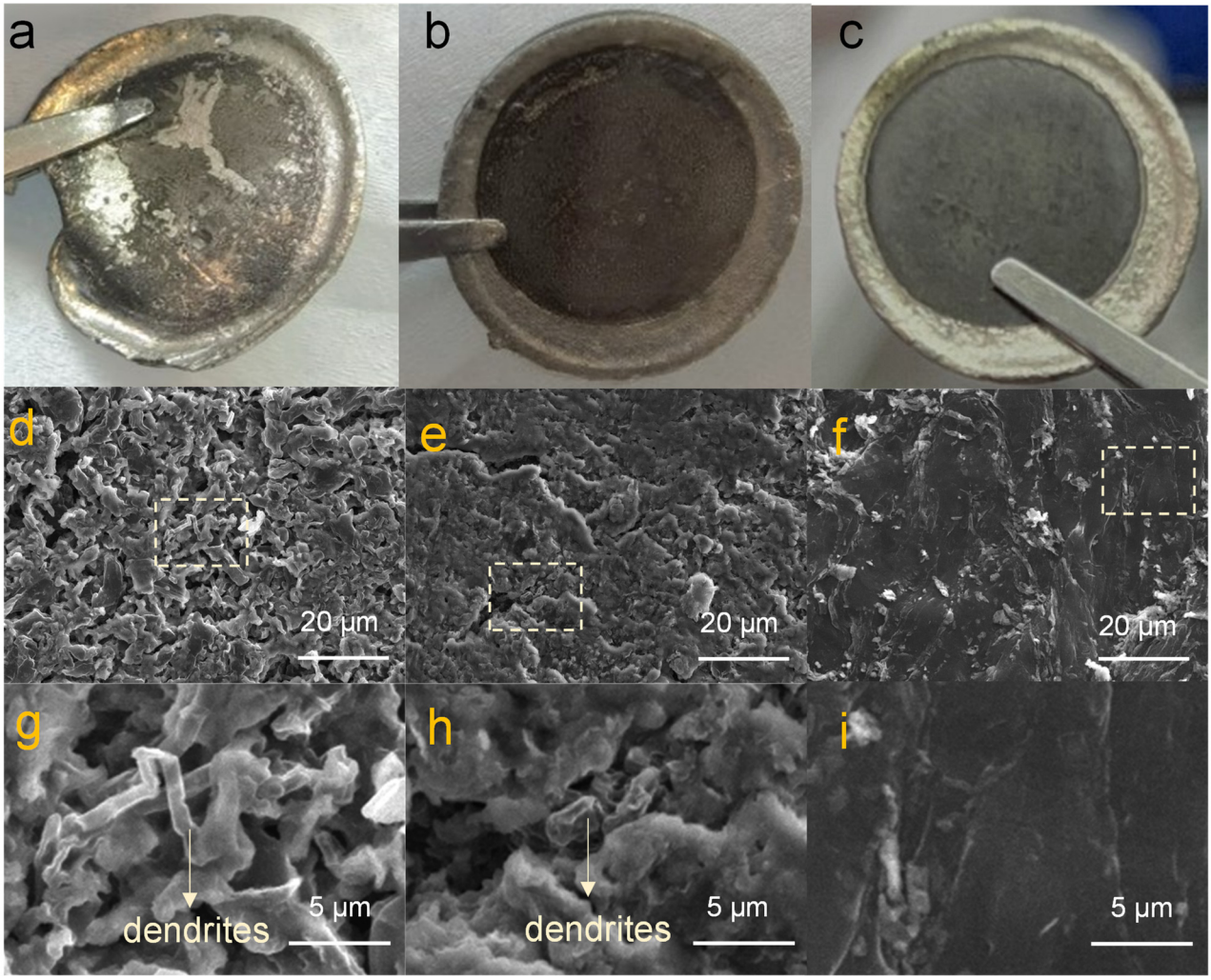

Figure S20. Digital photos as well as the SEM images of the Li metals retrieved from the cycled Li|NCM622 cells using (a, d, g) 2.6 M LiTFSI-DOL-TTE, (b, e, h) 1.3 M LiTFSI+1.3 M LiFSI-DOL-TTE, and (c, f, i) Hybrid-DOL/PDOL-TTE.

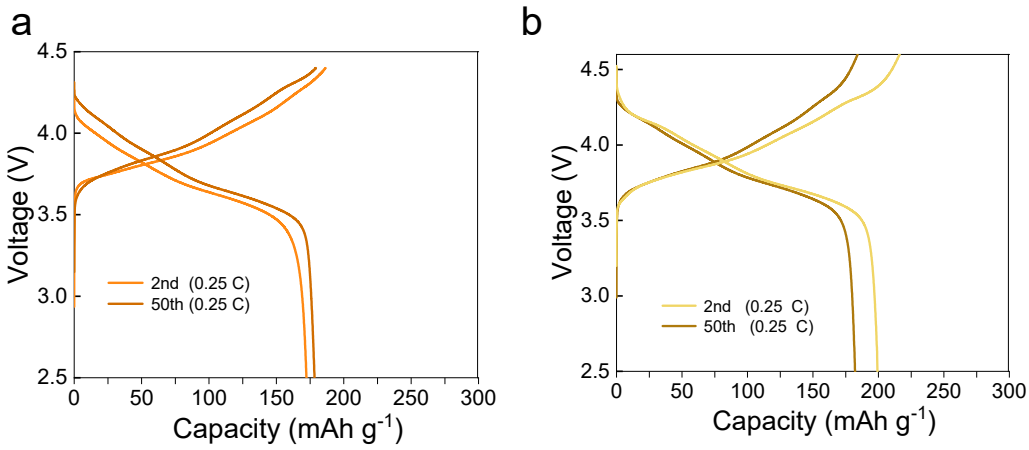

Figure S21. Voltage profiles of Li|NCM811 cells cycled using Hybrid-DOL/PDOL-TTE from (a) 2.5-4.4 V and (b) 2.5-4.6 V.

According to the reviewer's suggestion, we have supplemented the Li|NCM811 cell tests using our Hybrid-DOL/PDOL-TTE electrolyte. When the cutoff voltage is 4.4 V, the capacity of the Li|NCM811 cell remains stable at around 172.3 mAh g^{-1} after 50 cycles. After further increasing the cutoff voltage to 4.6 V, a high specific capacity close to 200 mAh g^{-1} can be achieved at 0.25 C and only a slight decay is observed after 50 cycles.

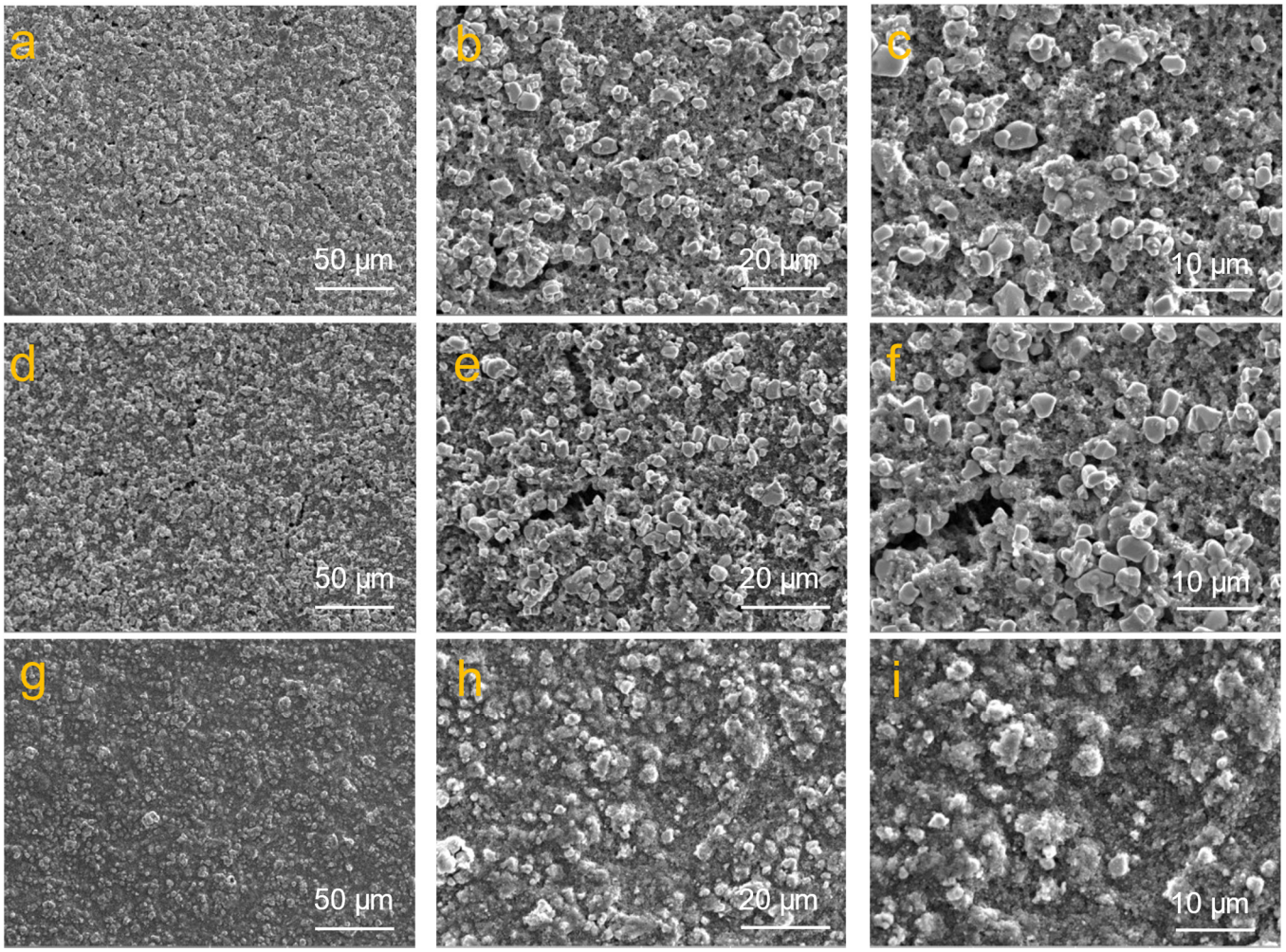

Figure S22. SEM images of the NCM622 cathodes retrieved from the cycled Li|NCM622 cells using (a-c) 2.6 M LiTFSI-DOL-TTE, (d-f) 1.3 M LiTFSI+1.3 M LiFSI-DOL-TTE, and (g-i) Hybrid-DOL/PDOL-TTE.

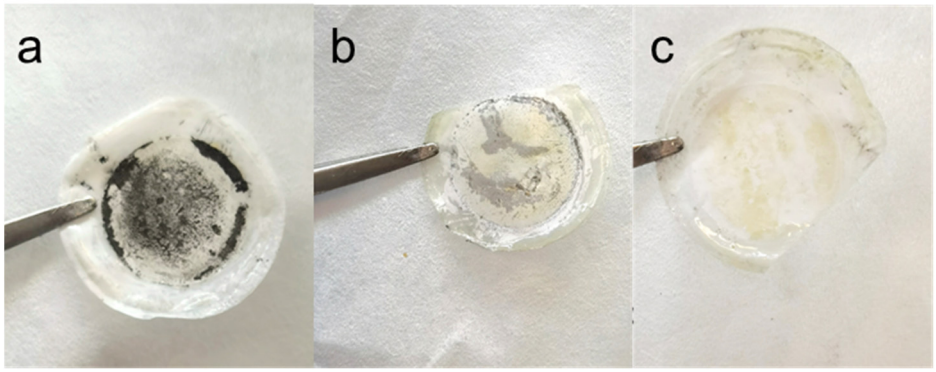

Figure S23. Digital photos of the separators retrieved from the cycled Li|NCM622 cells using (a) 2.6 M LiTFSI-DOL-TTE, (b) 1.3 M LiTFSI+1.3 M LiFSI-DOL-TTE, and (c) Hybrid-DOL/PDOL-TTE.

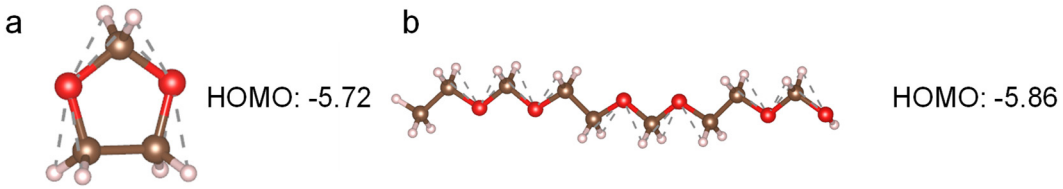

Figure S24. HOMO energy levels of (a) DOL and the polymerized chain-like ether when (b) n = 3 (n is the degree of polymerization) (unit: eV).

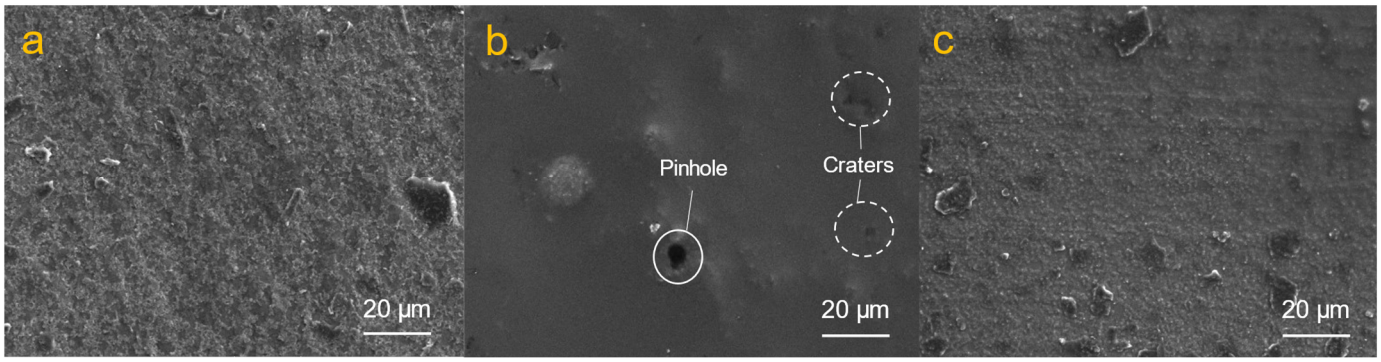

Figure S25. SEM images of (a) the pristine Al-C foil and the (b) Al-C current collector retrieved from the cycled Li|NCM622 cells using (b) 1.3 M LiTFSI+1.3 M LiFSI-DOL-TTE and (c) Hybrid-DOL/PDOL-TTE.

Figure S26. Photo image of 20-μm Li foil.

Table S1. Ionic conductivities of different electrolytes.

Electrolytes	Sigma (mS cm^{-1})
2.6 M LiTFSI-DOL-TTE	3.8
Hybrid-DOL/PDOL-TTE	2.8
1.3 M LiTFSI+1.3 M LiFSI-DOL-TTE	8.9

Table S2. Frequencies of all possible ion-solvent configurations in various electrolytes.

2.6 M LiTFSI-DOL-TTE			1.3 M LiTFSI+1.3 MLiFSI-DOL-TTE				Hybrid-DOL/PDOL-TTE				
TFSI	DOL	PROBABLITY	TFSI	FSI	DOL	PROBABLITY	TFSI	FSI	DOL	PolyDOL	PROBABLITY
2	3	35.7075	2	1	2	16.74875	2	1	1	0	9.6075
3	2	19.87625	1	2	2	15.3925	1	1	3	0	8.98625
2	2	16.855	1	1	3	12.00625	1	2	2	0	8.6175
3	1	7.4475	0	2	3	6.07	1	1	2	1	7.89625
1	4	6.34	1	2	1	5.45625	1	1	2	0	7.13375
3	3	4.6975	1	2	3	5.44	0	2	3	0	5.72375
1	3	4.05	1	0	4	4.7225	1	1	1	1	4.08875
2	4	3.92375	0	3	2	4.63	0	1	4	0	3.7275
2	1	0.54625	2	0	3	3.845	1	0	4	0	3.20375
			2	1	1	3.11	1	2	3	0	2.99125
			1	1	4	2.38	0	1	1	2	2.50875
			1	0	3	2.36875	1	0	1	1	2.49625
			1	1	2	2.31625	1	0	2	2	2.41125
			2	0	4	1.94	0	2	4	0	2.3875
			0	1	4	1.72625	3	1	0	1	2.3775
			0	3	3	1.72	1	2	2	1	2.33875
			2	2	1	1.64625	2	0	1	2	2.22
			0	2	2	1.27	2	2	1	0	2.0625
			2	1	3	1.20125	1	2	1	1	1.99375
			3	1	1	0.91125	0	3	1	0	1.885
			3	1	2	0.89375	0	2	2	0	1.85625
			0	2	4	0.79375	1	0	3	0	1.73875
			1	3	1	0.7425	2	1	2	0	1.71875
			3	0	2	0.645	1	0	2	1	1.5425
			1	0	5	0.54875	1	0	3	1	1.23875
							0	1	3	0	1.135
							3	1	1	0	1.0925
							1	1	1	2	0.91875
							1	2	0	1	0.66375
							0	3	2	0	0.615

Based on Table S3 and Table S4, we can conclude that the total frequencies of the configurations with a high anion-solvent ratio (ASR) in Hybrid-DOL/PDOL-TTE is far higher than that in 2.6 M LiTFSI-DOL-TTE and 1.3 M LiTFSI+1.3 M LiFSI-DOL-TTE. These configurations could lead to effective passivation of the anode and cathode with the formation of rich inorganics.

Table S3. Statistic of the solvation configurations with high ASRs or low LUMO/HOMO.

Total frequencies (%) of the given configurations (ASR means anion to solvent ratio)				
	ASR ≥ 2	**ASR ≥ 3**	**ASR = 4**	**Frequency of configurations in Table S4**
2.6 M LiTFSI-DOL-TTE	7.99	7.44	0	0
1.3 M LiTFSI+1.3 M LiFSI-DOL-TTE	12.76	11.87	3.3	11.86
Hybrid-DOL/PDOL-TTE	19.41	17.69	5.53	15.27

Table S4. Solvation configurations with low LUMO and HOMO.

Possible configurations with extremely low LUMO/HOMO			
TFSI	**FSI**	**DOL**	**LUMO/HOMO (eV)**
2	2	1	-1.37/-7.14
0	3	1	-1.50/-7.37
3	1	1	-1.22/-6.90
1	2	1	-1.43/-7.22
2	1	1	-1.35/-7.03
1	3	1	-1.48/-7.18

Table S5. Li anode performance comparison in various advanced electrolytes.

Literature	CE	Operation duration (Cycles)	Salt to solvent ratio	Areal capacity (mAh cm^{-2}) Current density (mA cm^{-2})
Energy Environ. Sci. **13**, 212-220 (2020).	99.03%	350	~1:2.8	0.5,0.5
Energy Environ. Sci. **14**, 3510-3521(2021).	<98.1%	250	~1:7	0.5,0.5
Science Bulletin **66** 897–903 (2021).	99.1%	450	1:3.25	1.0,1.0
Adv. Funct. Mater. 31, 2005991. (2021)	99.3%	500	1:1.2	1.0,1.0
Joule **3**,1662–1676 (2019)	99.3%	300	1:1.2	0.5,1.0
J. Am. Chem. Soc. 2021, 143, 18703−18713.	99.25%	800	1:2.1	0.5,1.0
Nat Energy 3, 674–681 (2018).	99%	140	1:2.0	0.2,1.0
Proc. Natl. Acad. Sci. U. S. A. **115** (6) 1156-1161 (2018)	98.7%	400	1:1.95	0.25,0.5
Chem **4**, 174–185 (2018)	99.3%	250	~1:1.05	0.2,1.0
This work	**99.2%**	**945**	**~1:3.6**	**1.0,1.0**

Table S6. Cathode performance comparison in various ether-based electrolytes.

Literature	CE	Retention	Decay rate (per cycle)	Maximum operating voltage	Salt to solvent ratio	Status
Nat. Energy **3**, 739–746 (2018).	N.A.	78.9% after 500 cycles	0.042%	4.3 V	1:1.5	Liquid
Nat. Energy **4**, 796–805 (2019).	99.7%	80% after 300 cycles	0.067%	4.4 V	>1:2	Liquid
Proc. Natl. Acad. Sci. U. S. A. **118** (9), 2020357118 (2021)	99.8%	80% after 300 cycles	0.067%	4.4 V	1:1.2	Liquid
Joule **3**,1662–1676, (2019).	99.77%	87% after 300 cycles	0.043%	4.5 V	1:1.2	Liquid
Nano Energy **96**,107102 (2022).	N.A.	80% after 300 cycles	0.067%	4.6 V	>1:1.2	Liquid
Energy Environ. Sci. **12**, 780—794 (2019)	N.A.	88% after 300 cycles	0.040%	4.4 V	1:1.6	Liquid
Sci. Adv. **4**, eaat5383 (2018)	N.A. for NCM cathode	10 cycles (NCM622)	N.A. (Fast decay)	4.3 V	≈1: 4	Solid polymer electrolyte (DOL-based)
Energy Environ. Sci. 14, 3510-3521(2021).	N.A. for NCM cathode	≈80% after 200 cycles	0.050%	4.3 V	≈1: 7	Solid polymer electrolyte (DOL-based)
Adv. Mater. **32**, 1905629 (2020) .	N.A. for NCM cathode	69 cycles (NCM622)	N.A. (Fast decay)	4.3 V	≈1: 7	Solid polymer electrolyte (DOL-based)
Nat Energy 4, 365–373 (2019).	N.A. For NCM cathode	5 cycles (NCM622)	N.A. (Fast decay)	4.2 V	≈1: 7	Solid polymer electrolyte (DOL-based)
This work	**99.87 %** (after 100th cycle at 2.5-4.4 V)	86% after 300 cycles (2.5-4.4 V)	0.046% (2.5-4.4 V)	**4.6 V**	**1:3.6**	**Liquid** (DOL-based)

Only typical high-voltage cathode including LCO, NCM, and NCA are considered in above-literature if not specially specified;

Table S7. Component details of the 20-μm Li|NCM622 pouch cell.

Pouch cell overview	
Cathode	14.8 mg cm^{-2}
Anode	1.3 mg cm^{-2}
Separator (Celgard 3501)	1.02 mg cm^{-2}
Electrolyte	11 mg cm^{-2}
Al foil	2.1 mg cm^{-2}
Binder PVDF	1.36 mg cm^{-2}
Conductive Carbon	1.36 mg cm^{-2}
Total mass	32.94 mg cm^{-2}
Areal capacity	~3.0 mAh cm^{-2}
Energy density based on electrodes	**710 Wh kg^{-1}**
Energy density	**347.1 Wh kg^{-1}**

Table S8. Component details of the 20-μm Li|NCM622 pouch cell.

Literature	Cycle Life	N/P ratio	Cell type; Operation voltage(V)	Energy density (Wh kg^{-1})
Angew.Chem. 2020, 132,3278 –3283	60	1.6	Li|NCM523; 2.8-4.3	340
Angew. Chem. Int. Ed. 2018, 57,1 – 6	125	> 5.0	Li|LFP; 2.8-4.3	*None*
Angew. Chem. 2022, 134, e202116214	100	2.5	Li|NCM622;3.0-4.2	300
Nat. Energy 2019, 4, 551–559	50	2.6	Li|NCM622; 2.8-4.4	300
Adv. Energy Mater. 2019, 9, 1900257	27	>>10	Li|NCM622; 2.8-4.2	*None*
Joule 2019, 3, 1094–1105, April 17	15	2.86	Li|NCM622; 2.7-4.4	≈300
Joule 2019, 3, 1094–1105, April 17	40	≈4	Li|NCM622; 2.7-4.4	<300
Joule 2019, 3, 1094–1105, April 17	75	≈7.3	Li|NCM622; 2.7-4.4	<<300
Energy Storage Materials, 2020, 32, 55–64	50	*Excessive Li*	Li|LFP; 2.5-4.0	*None*
Nat. Commun. 2022, 13, 1510	100	*Excessive Li*	Li|NCM811; 2.7-4.4	*None*
Nano Energy 2022, 93, 106805	60	*Excessive Li*	Li|NCM811; up to 4.3	≈350
Nano Energy 2022, 96,107102	20	1.0	Li|NCM622; 2.5-4.6	≈350
This work	60	1.7	2.5-4.6 V	347.1

References

[1] H. J. C. Berendsen, J. P. M. Postma, W. F. van Gunsteren, A. DiNola and J. R. Haak, *J. Chem. Phys.*, 1984, **81**, 3684–3690.

[2] W. D. Cornell, P. Cieplak, C. I. Bayly, I. R. Gould, K. M. Merz, D. M. Ferguson, D. C. Spellmeyer, T. Fox, J. W. Caldwell and P. A. Kollman, *J. Am. Chem. Soc.*, 1995, **117**, 5179–5197.

[3] Lu T, Chen F. Multiwfn: a multifunctional wavefunction analyzer. *J. Comput. Chem.*, 2012, **33**(5): 580-592.

[4] Tian Lu, Sobtop, Version [1.0(dev2)], http://sobereva.com/soft/Sobtop

[5] T. Darden, D. York and L. Pedersen, J. Chem. Phys., 1993, **98**, 10089–10092.

[6] Allouche, A. R. *J. Comput. Chem*., 2011, **32**, 174−182.

[7] Yu Z, Wang H, Kong X, et al. *Nat. Energy*, 2020, **5**(7): 526-533.

[8] Chen Y, Yu Z, Rudnicki P, et al. *J. Am. Chem. Soc.*, 2021, **143**(44): 18703-18713.

[9] Hafner J. J. Comput. *Chem.*, 2008, **29**(13): 2044-2078.

[10] Hammer B, Hansen L B, Nørskov J K. *Phys. Rev. B*, 1999, **59**(11): 7413.